Fading correlation and analytical performance evaluation of the space-diversity free-space optical communications system

G. Yang[1], M.A. Khalighi[2], S. Bourennane[2], Z. Ghassemlooy[3]

[1] College of Communication Engineering, Hangzhou Dianzi University, Hangzhou, P. R. China

[2] Institut Fresnel, UMR CNRS 7249, Ecole Centrale Marseille, Marseille, France

[3] Optical Communications Research Group, Faculty of Engineering and Environment, Northumbria University, Newcastle Upon Tyne, UK

E-mail: ali.khalighi@fresnel.fr

Abstract. This paper investigates fading correlation in space-diversity free-space optical (FSO) communication systems and its effect on the link performance. We firstly evaluate the fading correlation in multiple-aperture FSO systems using wave-optics simulations. The influence of different system parameters including the link distance and aperture spacing is illustrated under realistic beam propagation conditions. In particular, we show that at relatively large link distances where the scattering disk is much larger than the receiver aperture size, the fading correlation coefficient is almost independent of the apertures' diameter and depends only on the apertures' edge separation. To investigate the impact of fading correlation on the system performance, we propose an analytical approach to evaluate the performance of the space-diversity FSO system over correlated Gamma-Gamma ($\Gamma\Gamma$) fading channel. Our approach is based on approximating the sum of arbitrarily correlated $\Gamma\Gamma$ random variables (RVs) by an α-μ distribution. To validate the accuracy of this method, we evaluate the average bit-error-rate (BER) performance for the case of multiple-aperture FSO system and compare it with the BER results obtained via Monte-Carlo simulations.

1. Introduction

Under clear weather conditions, one of the main challenges in free-space optical (FSO) communications is to reduce the effect of atmospheric turbulence that can severely degrade the system performance, especially for relatively long link distances [1]. Efficient mitigation of the resulting channel fading can be obtained via spatial diversity, which has been widely adopted for applications in radio and microwave frequency bands. This can be realized by employing multiple apertures at the receiver and/or multiple beams at the transmitter [2–7]. However, such techniques lose their efficacy under the conditions of correlated fading on the underlying sub-channels, i.e., channels between pairs of transmit-receive apertures [8]. In particular, under strong turbulence conditions, the required spacing between the apertures at the receiver and/or between the laser beams at the transmitter is usually too large to ensure uncorrelated fading and unfeasible for a practical design [5, 6, 9, 10].

In most previous works reported on space-diversity FSO systems, the fading correlation is either ignored or studied considering a simplified channel model (see [4, 8, 11, 12]). In this paper, we consider the Gamma-Gamma ($\Gamma\Gamma$) distribution that is widely adopted for modeling the terrestrial FSO channel due to its excellent agreement with the experimental data over all turbulence conditions [2]. Under the *ideal* conditions of independent $\Gamma\Gamma$ fading, the performance of multiple-aperture FSO systems was studied in [2, 5]. Also, two approximations to the sum of independent $\Gamma\Gamma$ random variables (RVs), based on $\Gamma\Gamma$ [13] and α-μ [14] distributions, were used in the performance analysis of space-diversity FSO systems.

Concerning correlated fading conditions, multi-beam terrestrial and air-to-air FSO systems were studied in [6] and [15], respectively. In [6], multiple $\Gamma\Gamma$ channels were modeled by a single $\Gamma\Gamma$ distribution whose parameters were calculated by approximating the fading coefficients by correlated Gaussian RVs. However, when employed to predict the system performance, this solution cannot guarantee sufficient accuracy. In [15], approximate analytical expressions based on numerical fitting were proposed to determine the parameters of $\Gamma\Gamma$ model taking the fading correlation into account. However, the proposed expressions depend on the underlying air-to-air system structure and cannot directly be used to accurately evaluate the BER in general. Also, a multivariate $\Gamma\Gamma$ model with the exponential correlation was proposed in [16], but this correlation model is not suitable for most FSO system configurations. In a recent work [17], we proposed the α-μ approximation to the sum of two correlated $\Gamma\Gamma$ RVs for evaluating the performance of a dual-diversity FSO system.

In this paper, we firstly evaluate the fading correlation in a multiple-aperture link using wave-optics simulations, and study the impact of different system parameters on the link average correlation coefficient. In contrast to a similar study presented in [6] for a four-beam single-aperture FSO system, we consider here more practical cases for the receiver aperture size and link span. To consider different turbulence regimes, we use different link spans and fix the turbulence strength parameter C_n^2. Although, in

general, C_n^2 depends on the link distance [18] (because it is altitude dependent), for horizontal FSO paths that we consider in this work, C_n^2 can be considered as constant (irrespective of the link span), which is usually referred to as homogeneous turbulence conditions [19]. Alternatively, one may consider a fixed link span and consider different C_n^2 values (that could correspond to different moments during the daytime [20, 21], for example) as done in [6].

Note that in a previous work [22] we simply illustrated the effect of link distance and aperture separation on the fading correlation coefficient and focused on the generation of correlated $\Gamma\Gamma$ RVs in order to evaluate the system BER performance via Monte Carlo simulations. In contrast to [22], here we present a comprehensive investigation of the impact of link span, aperture diameter, and aperture separation on the fading correlation. Furthermore, we explain the presented results using the scintillation theory and by ascribing the fading correlation to small- and large-scale fading components. Afterwards, we propose an analytical approach to investigate the impact of fading correlation on the system BER. For this purpose, we extend the α-μ approximation method proposed in [17] to the case of multiple diversity by approximating the sum of arbitrarily correlated multiple $\Gamma\Gamma$ RVs by an α-μ distribution. As a matter of fact, the proposed method in [17] was based on the joint moments of Gamma-distributed RVs. Therein, we could only find the joint moments of two correlated Gamma RVs in a closed-form formula. It is worth mentioning that we cannot obtain the joint moments of more than two correlated Gamma RVs by the same method. To the best of our knowledge, there is no previous reported work on the analytical performance evaluation of multiple-diversity FSO systems over arbitrarily correlated $\Gamma\Gamma$ fading channels. For this, we derive joint moments of correlated multiple Gamma RVs based on the moment generating function (MGF) (as introduced in [23]), and then extend the α-μ approximation method to deal with the arbitrarily correlated multiple $\Gamma\Gamma$ RVs.

The remainder of the paper is organized as follows. After presenting the main assumptions and a brief introduction on wave-optics simulation tool in Section 2, we explain our method of approximating the sum of correlated $\Gamma\Gamma$ RVs by α-μ distribution in Section 3. Then, we provide some numerical results to evaluate fading correlation by considering the case study of a receive-diversity FSO system in Section 4. The accuracy of α-μ approximation is next investigated in Section 5, where we also contrast the corresponding analytical performance results with those obtained via Monte Carlo simulations. Lastly, Section 6 concludes the paper.

2. General assumptions and wave-optics simulations

We assume that the transmitter and the receiver are perfectly aligned. Also, we reasonably assume that the parameters of the $\Gamma\Gamma$ model are the same for all underlying sub-channels.

We use the split-step Fourier-transform algorithm for the numerical simulation of optical wave propagation, where the effect of atmospheric turbulence along the

Table 1. Scale sizes for different Z.

Z(km)	σ_R^2	ℓ_1(mm)	ℓ_2(mm)
1.0	1.29	21.0	11.7
2.0	4.61	14.1	34.9
3.0	9.70	11.2	66.3
4.0	16.43	9.4	104.7
5.0	24.74	8.3	149.4

propagation path is taken into account by considering a set of random phase screens [24]. For each phase screen, we generate random harmonic amplitudes over an $N_g \times N_g$ grid in the spectral domain based on the modified von Kármán power spectrum, and then, take the inverse 2-D discrete Fourier transform to obtain the phase fluctuations [2]. To achieve sufficient accuracy at very low spatial frequencies, we perform a spectral correction in the subharmonic regime and also use the two-dimensional super-Gaussian function to avoid energy leakage at the edge of each screen [24]. To obtain accurate results, the grid spacing, grid size parameter N_g, and the number of phase screens are set appropriately (see [22] for details). Calculating the transmitted and the received intensities on each receiver aperture, we obtain the channel fading coefficients and then calculate the Pearson correlation coefficient among them [22].

For the later use, we have provided in Table 1 the spatial coherence radius ℓ_1 [2] and the scattering disk ℓ_2 [2], for different link distances Z together with Rytov variance σ_R^2.

3. α-μ approximation method

3.1. $\Gamma\Gamma$ *and* α-μ *distributions*

Using the $\Gamma\Gamma$ model, we consider the normalized received intensity at a receiver aperture I as the product of two independent Gamma RVs, X and Y, which represent the irradiance fluctuations arising from large- and small-scale turbulence, respectively. The PDF of I is [2]:

$$f_I(i) = \frac{2(ab)^{(a+b)/2}}{\Gamma(a)\Gamma(b)}\, i^{\frac{(a+b)}{2}-1} K_{a-b}(2\sqrt{a\,b\,i}),\ i \geq 0, \tag{1}$$

where a and $b \geq 0$ denote the effective numbers of large- and small-scale turbulence eddies, respectively, which can be directly obtained from the link's parameters [2]. Also, $\Gamma(.)$ is the Gamma function and $K_\upsilon(.)$ is the modified Bessel function of the second kind and order υ. The n^{th} moment of I is [13]:

$$\mathrm{E}\{I^n\} = \frac{\Gamma(a+n)\,\Gamma(b+n)}{\Gamma(a)\,\Gamma(b)}\,(ab)^{-n}, \tag{2}$$

where $\mathrm{E}\{.\}$ denotes the expected value.

The reason behind choosing the α-μ distribution, which is also known as generalized Gamma, is that it is a flexible distribution that can be reduced to several simplified distributions such as Gamma, Nakagami-m, exponential, Weibull, one-sided Gaussian, and Rayleigh [25, 26]. Let us denote the α-μ distributed RV by R. The PDF of R is given by [26]:

$$f_R(r) = \frac{\alpha\,\mu^{\mu}\,r^{\alpha\mu-1}}{\hat{r}^{\alpha\mu}\,\Gamma(\mu)} \exp\left(-\mu\,\frac{r^{\alpha}}{\hat{r}^{\alpha}}\right),\ r>0, \tag{3}$$

where $\alpha > 0$, $\hat{r} = \sqrt[\alpha]{\mathrm{E}\{R^{\alpha}\}}$, and μ is the inverse of the normalized variance of R^{α}, defined as:

$$\mu = \frac{\left(\mathrm{E}\{R^{\alpha}\}\right)^2}{\mathrm{Var}\{R^{\alpha}\}}, \tag{4}$$

and Var{.} denotes variance. The n^{th} moment of R is given by [26]:

$$\mathrm{E}\{R^n\} = \hat{r}^n\,\frac{\Gamma(\mu+n/\alpha)}{\mu^{n/\alpha}\,\Gamma(\mu)}. \tag{5}$$

3.2. α-μ approximation to sum of multiple correlated $\Gamma\Gamma$ RVs

Let us consider the general case of space-diversity FSO systems with L diversity branches. The normalized fading coefficient of the i^{th} sub-channel is denoted by I_i, which is governed by $\Gamma\Gamma$ distribution. We approximate the sum $I_{\text{sum}} = \sum_{i=1}^{L} I_i$ by an α-μ RV R by setting equal the corresponding first three moments. For the general case of an M-beam N-aperture FSO system, I_{sum} corresponds to the received signal intensity after equal gain combining (EGC) [8] when repetition coding (RC) [4] is performed at the transmitter. In this case, we have $L = MN$. (Note that EGC has a performance very close to the optimal maximal ratio combining [8, 11], and RC has been shown to be the quasi-optimal transmission scheme in transmit-diversity FSO systems [27, 28].) Then, using the moment-matching method [14, 17], we have:

$$\begin{cases} \mathrm{E}\{R\} = \mathrm{E}\{I_{\text{sum}}\} = \mathrm{E}\left\{\sum\limits_{i=1}^{L} X_i Y_i\right\}, \\ \mathrm{E}\{R^2\} = \mathrm{E}\{I_{\text{sum}}^2\} = \mathrm{E}\left\{\left(\sum\limits_{i=1}^{L} X_i Y_i\right)^2\right\}, \\ \mathrm{E}\{R^3\} = \mathrm{E}\{I_{\text{sum}}^3\} = \mathrm{E}\left\{\left(\sum\limits_{i=1}^{L} X_i Y_i\right)^3\right\}. \end{cases} \tag{6}$$

We notice from (6) that we need the first, second, and third moments of I_{sum}. The general expression of the n^{th} moment of I_{sum} is given in (7), on the top of this page, where $v_1, v_2, \cdots, v_L$, and n are non-negative integers [29]. One notes that $\mathrm{E}\{I_{\text{sum}}^n\}$ depends on the joint moments of the Gamma RVs X_i and Y_i. The first, second, and third joint moments of X_i and Y_i can in turn be calculated using (A.5), (A.6) and (A.17), given in the appendix. Then, setting equal the first three moments of I_{sum}

$$\mathrm{E}\left\{I_{\mathrm{sum}}^{n}\right\} = \mathrm{E}\left\{\left(\sum_{i=1}^{L} I_i\right)^{n}\right\} = \mathrm{E}\left\{\left(\sum_{i=1}^{L} X_i Y_i\right)^{n}\right\} =$$
$$\sum_{v_1=0}^{n}\sum_{v_2=0}^{v_1}\cdots\sum_{v_{L-1}=0}^{v_{L-2}}\binom{n}{v_1}\binom{v_1}{v_2}\cdots\binom{v_{L-2}}{v_{L-1}}$$
$$\times\mathrm{E}\left\{X_1^{n-v_1}X_2^{v_1-v_2}\cdots X_L^{v_{L-1}}\right\}\mathrm{E}\left\{Y_1^{n-v_1}Y_2^{v_1-v_2}\cdots Y_L^{v_{L-1}}\right\} \quad (7)$$

(using (7)) and R (using (5)), we calculate the three parameters of the approximate α-μ distribution from (6).

Since it is difficult to obtain a closed-form solution for these parameters due to nonlinear functions in (6), we use numerical methods to calculate α, μ and $\hat{r}$ (more specifically, we use the *fsolve* function of MATLAB) .

Note that to calculate the first three moments of X_i and Y_i, we need in (A.5), (A.6), and (A.17), the correlation coefficients between X_i and X_j and those between Y_i and Y_j. These coefficients can be obtained from the correlation coefficients between I_i and I_j (calculated via wave-optics simulations), as we will explain in Section 5.1.

Finally, note that for the simple case of a single-beam single-aperture FSO system, where $L = 1$, the moment matching of (6) can simply be done using (2) and (5).

4. Evaluating fading correlation

4.1. Numerical simulations' parameters

We consider a diverging Gaussian beam operating at $\lambda = 1550\,\mathrm{nm}$ with the beam waist $W_0 = 1.59\,\mathrm{cm}$ and a curvature radius of the phase front $F_0 = -69.9\,\mathrm{m}$, corresponding to a beam divergence $\theta_{\mathrm{div}} = |2W_0/F_0|$ of 0.46 mrad (see Fig. 1(a)). Concerning the FSO channel, we consider the refractive-index structure parameter $C_n^2 = 6.5\times10^{-14}\,\mathrm{m}^{-2/3}$, the inner scale $l_0 = 6.1\,\mathrm{mm}$, and the outer scale of turbulence $L_0 = 1.3\,\mathrm{m}$. Note that these transmitter and turbulence parameters correspond to the experimental works reported in [30].

Without loss of generality, we consider a triple-aperture receiver as a case study (see Fig. 1(b)). Here, due to the specific structure of the receiver, we should have equal correlation coefficients between the three pairs of sub-channels because we have the same separation among the corresponding apertures. Therefore, to get more accurate results, we average the corresponding calculated correlation coefficients and denote it by ρ. We express the apertures' diameter and their center and edge separations by D_R, Δ_C and Δ_E, respectively. We limit the total receiver diameter to 250 mm for practical manufacturing reasons.

For wave-optics simulations, the grid spacing is set to 2 mm, and N_g as well as the number of phase screens are appropriately set depending on the link span Z.

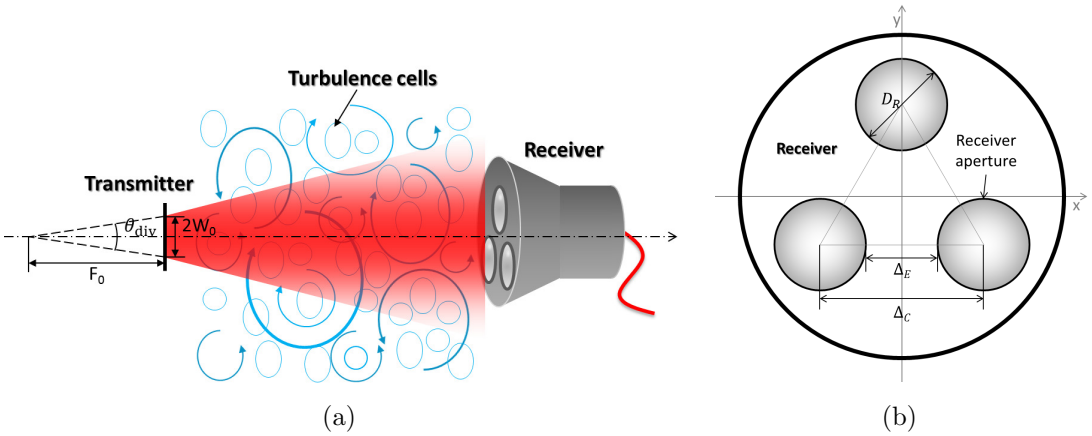

Figure 1. The schematic of the triple-aperture FSO link (a) and its receiver geometry (b).

To consider practical scenarios, we consider relatively large apertures and long link spans up to a few kilometers, which leads to too time- and memory-consuming wave-optics simulations. Nevertheless, the number of samples used for calculating the fading correlation coefficients was at least 10^4.

4.2. Study of fading correlation

4.2.1. Fixed aperture diameter D_R Let us first fix the aperture size and investigate the effect of Z and Δ_C on ρ. We have shown in Fig. 2 plots of ρ as a function of Δ_C for $D_R = 50\,\text{mm}$ and a range of Z. We have also shown on each calculated point the error bar corresponding to one standard deviation of the estimation error. As explained in [2], the reason behind the negative ρ values is that the covariance function of irradiance fluctuations follows a Bessel function of the first kind and zero order, which has a tail oscillating around zero. This has also been verified by experiments in [31], and we confirmed it by wave-optics simulations as well.

We notice from Fig. 2 that, as expected, ρ decreases by increasing Δ_C. Also, ρ is larger for increased Z. The reason is that, with increased Z, there are more atmosphere eddies that affect the three apertures at the same time. For example, the required Δ_C to have almost uncorrelated fading is about 65 and 100 mm, for $Z = 1$ and 2 km, respectively. The interesting point is that we notice a non-homogenous increase in ρ with respect to Z. In fact, by increasing Z, ℓ_1 decreases whereas ℓ_2 increases. This means that due to aperture averaging, the large-scale turbulence becomes more and more predominant. As fading correlation arises partly from small-scale and partly from large-scale turbulence, for $Z \gtrsim 3\,\text{km}$ where D_R is quite smaller than ℓ_2 and larger than ℓ_1, the increase in ρ by increasing Z becomes relatively slower.

Note that in [22], we had set $l_0 = 4.6\,\text{mm}$ with the other parameters specified here. Comparing the presented results with those of [22], we conclude that l_0 has a negligible influence on the correlation among sub-channels.

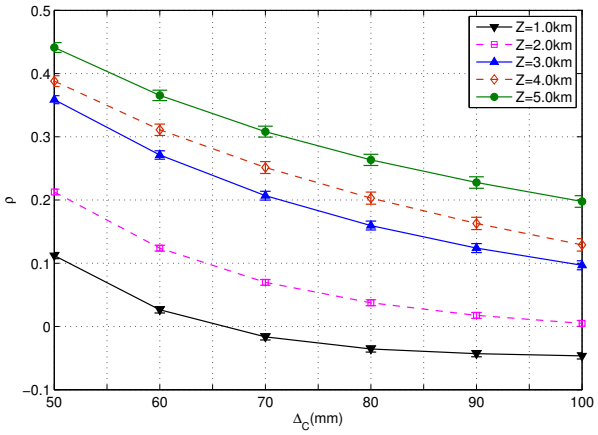

Figure 2. Average correlation coefficient versus aperture spacing in a triple-aperture FSO system for different link distances. $D_R = 50\,\text{mm}$.

4.2.2. Fixed link distance Z Let us now fix Z and see the influence of D_R and Δ_C on ρ. Figure 3 shows plots for ρ versus Δ_C for $Z = 2$ and 5 km and a range of D_R. Remember that we limit the total receiver aperture diameter to 250 mm, which confines the choice of Δ_C for a given D_R. From Fig. 3 we notice that ρ increases with D_R for a fixed Δ_C. In fact, for fixed Δ_C, a larger D_R leads to a larger aperture area and a smaller Δ_E (see Fig.1). So, there are more turbulent eddies that intervene at the same time in the scintillation corresponding to the different apertures. (For $Z = 2\,\text{km}$ and $\Delta_C \gtrsim 110\,\text{mm}$, ρ is too small and its dependence on D_R is not manifest.)

Let us now fix Δ_E to observe the effect of increasing D_R on ρ. We have rearranged the results of Fig. 3 in Fig. 4 in order to show plots of ρ as a function of D_R. Note that $\Delta_C = \Delta_E + D_R$, and hence, increasing D_R implies an increase of Δ_C for a given Δ_E. We notice that ρ monotonously decreases with increases in D_R. In fact, by increasing D_R, the apertures extend outward from the receiver center, therefore encountering more dissimilar scintillations, which results in a smaller ρ.

We notice from Fig. 4 that ρ is almost independent of D_R for sufficiently large Δ_E. To understand this point, we should recall that small scale fading originates mostly from turbulent eddies of size between l_0 and ℓ_1, and large-scale fading arises from turbulent eddies of size between ℓ_2 and L_0 [2]. Consider first the case of $Z = 5\,\text{km}$ in Fig. 4(b). From Table 1, we have $\ell_1 = 8.3\,\text{mm}$. Consequently, for $\Delta_E > 10\,\text{mm}$, dissimilar small-scale scintillations affect the different apertures and the fading correlation mostly arises from the large-scale fading. Since $\ell_2 = 149.4\,\text{mm}$, we receive almost identical large-scale fading for the different apertures when increasing D_R from 30 to 70 mm. Moreover, we cannot average over large-scale fading at each aperture. Consequently, ρ remains almost constant by increasing D_R. On the other hand, for $\Delta_E \lesssim 10\,\text{mm}$, the correlation will arise also from the small-scale fading; however, due to reduced small-scale fading effect because of aperture averaging by increasing D_R, ρ decreases only slightly by increasing D_R. Note that when Δ_E is sufficiently larger than ℓ_1, almost no correlation arises from

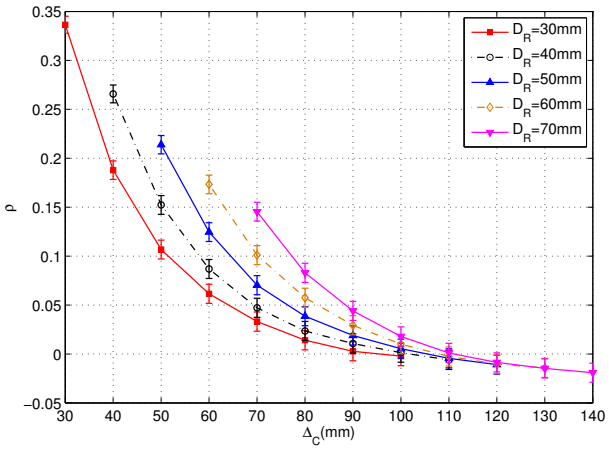

(a)

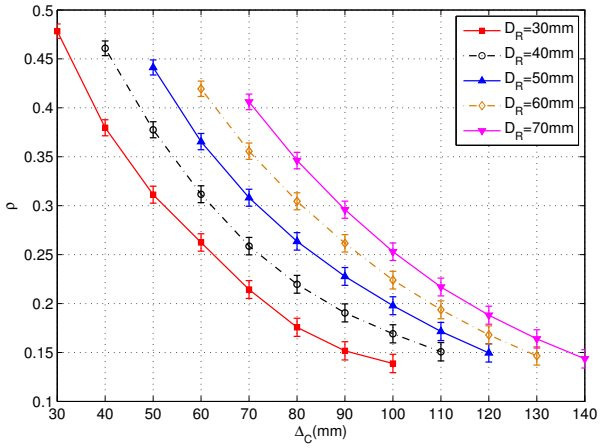

(b)

Figure 3. Average correlation coefficient for a (1×3) system versus the aperture spacing Δ_C for different D_R: (a) $Z = 2\,\text{km}$, (b) $Z = 5\,\text{km}$.

the small-scale turbulence and, hence, ρ is almost independent of D_R.

We conclude that for sufficiently large link distances, where $\ell_2 \gg D_R$, ρ practically depends on Δ_E and is almost independent of D_R. This can be important when designing a practical system.

Concerning the case of $Z = 2\,\text{km}$ in Fig. 4(a), here we have a larger ℓ_1 (14.1 mm) and a smaller ℓ_2 (34.9 mm), and, hence, we notice a more dependence of ρ on D_R.

5. Effect of fading correlation on BER performance

For analytical performance evaluation in the case of correlated fading, we use the α-μ approximation method, described in Section 3. Let us first investigate the accuracy of approximating the distribution of the sum of correlated multiple $\Gamma\Gamma$ RVs by an α-μ distribution.

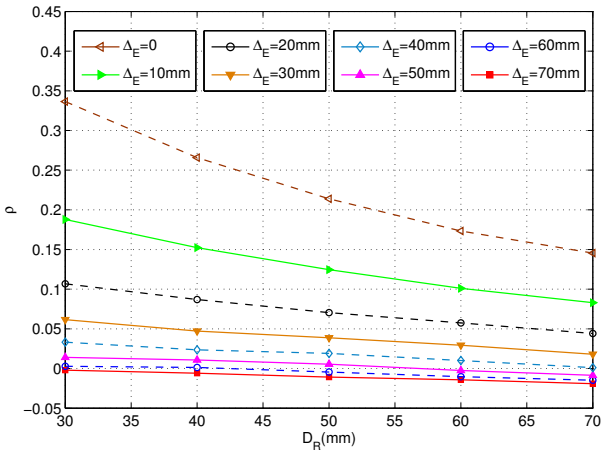

(a)

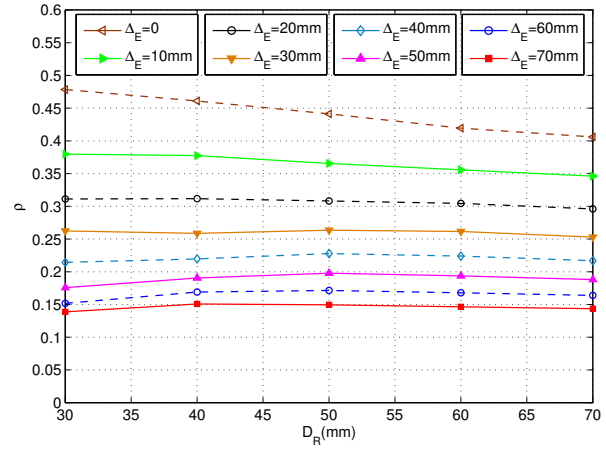

(b)

Figure 4. Average correlation coefficient for a (1×3) system versus D_R for different aperture side-spaces Δ_E: (a) $Z = 2\,\text{km}$, (b) $Z = 5\,\text{km}$.

5.1. Goodness-of-fit test for α-μ approximation

To validate the accuracy of the proposed approximation method, we use the well known Kolmogorov-Smirnov (KS) goodness-of-fit test [13,32,33]. We should calculate the KS test statistic T which represents the maximal difference between the cumulative distribution functions (CDFs) of I_{sum} and R. However, to obtain the CDF of I_{sum}, we need to randomly generate correlated $\Gamma\Gamma$ RVs.

5.1.1. Generating correlated $\Gamma\Gamma$ RVs To the best of our knowledge, there is no reported method to directly generate correlated $\Gamma\Gamma$ RVs. Here, we consider the fading correlation as arising partly from the large-scale and partly from the small-scale turbulence eddies and denote the corresponding correlation coefficients by ρ_X and ρ_Y, respectively. We

have [22]:

$$\rho = \frac{a\rho_{_X} + b\rho_{_X} + \rho_{_X}\rho_{_Y}}{a+b+1}. \tag{8}$$

Remember from Section 2 that we consider the same $\Gamma\Gamma$ fading parameters a and b for different sub-channels. From (8) and for a given ρ, mathematically, we have an infinite number of solutions for $\rho_{_X}$ and $\rho_{_Y}$. In a recent work [34], we have shown that we can practically neglect $\rho_{_Y}$ irrespective of turbulence conditions. Therefore, we generate independent small-scale fading coefficients and correlated Gamma-distributed large-scale fading coefficients with $\rho_{_X} = \rho\frac{a+b+1}{b}$ using the method proposed in [35].

5.1.2. KS test results We consider three multiple aperture FSO cases of (1×3), (1×4), and (1×6) systems. Due to the specific receiver geometry for the (1×3) system (see Fig. 1), we have equal correlation coefficients between each pair of sub-channels. Although the proposed α-μ approximation method can be applied to an arbitrary correlation model [33, 36, 37], for the sake of modeling simplicity, let us consider equal correlation coefficients between all sub-channel pairs for (1×4) and (1×6) configurations as well. In fact, this corresponds to the worst case correlation scenario [33]. We consider $Z = 2\,\text{km}$ and $D_R = 50\,\text{mm}$ and use the correlation coefficients from the results of wave-optics simulations in Fig. 3(a). For instance, we have $\rho_{_1} = 0.12$ and $\rho_{_2} = 0.21$, corresponding to the aperture edge separations of $\Delta_E = 10\,\text{mm}$ and 0, respectively.

To carry out the KS test, we have presented in Table 2(a) the T values for the considered correlation cases together with the uncorrelated fading case. These results have been averaged over 100 runs. To obtain these results, we have set the significance level to $\alpha = 5\%$ and generated $n = 10^4$ random samples I_{sum}, which corresponds to the critical value $T_{\max} \simeq \sqrt{-\frac{1}{2n}\ln\frac{\alpha}{2}} = 0.0136$ [13, 32]. (Note that this value is independent of the specific distribution.) This means that the hypothesis that the random samples I_{sum} belong to the approximate α-μ RV R is accepted with 95% significance when $T < T_{\max}$. The results in Table 2(a) show a good match between I_{sum} and R because all the values of T are smaller than $T_{\max}$. However, we notice that T increases with ρ, which means less accuracy of the approximation. We have also less accuracy for increased diversity order. We have further presented the p-values for the corresponding KS tests in Table 2(b). In fact, if the significance level α is smaller than p, then the null hypothesis is accepted under the significance level. We notice that all p-values are larger than α, which confirms the results in Table 2(a).

For the sake of completeness, we have also contrasted in Fig. 5 the probability density functions (PDFs) of I_{sum} and R for some cases considered in Table 2(a), where we notice a good fit between them. Lastly, we have provided in Table 3 the values of α, μ and $\hat{r}$ after α-μ approximation for the different case studies.

Table 2. KS test statistic T and p-value for $\alpha = 5\%$ and 10^4 samples.

(a) test statistic T

	(1×3)	(1×4)	(1×6)
$\rho = 0$	0.0083	0.0082	0.0088
ρ_1	0.0090	0.0089	0.0092
ρ_2	0.0096	0.0098	0.0101

(b) p-value

	(1×3)	(1×4)	(1×6)
$\rho = 0$	0.4702	0.5113	0.4261
ρ_1	0.4384	0.4596	0.3482
ρ_2	0.4101	0.3758	0.2729

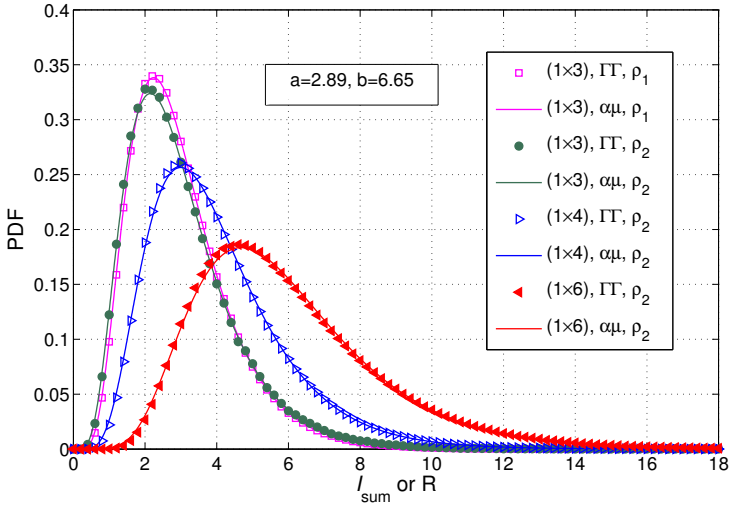

Figure 5. Contrasting the PDFs of the total received intensity I_{sum} obtained from Monte-Carlo simulations (using the ΓΓ model) and the corresponding α-μ approximation R with different fading correlation coefficients ρ.

Table 3. Values of α, μ and $\hat{r}$ for α-μ approximation.

	(1×3)	(1×4)	(1×6)
$\rho = 0$	$\alpha = 0.51$, $\mu = 21.79$ $\hat{r} = 2.87$	$\alpha = 0.50$, $\mu = 29.94$ $\hat{r} = 3.87$	$\alpha = 0.49$, $\mu = 46.49$ $\hat{r} = 5.86$
ρ_1	$\alpha = 0.40$, $\mu = 28.07$ $\hat{r} = 2.81$	$\alpha = 0.33$, $\mu = 52.00$ $\hat{r} = 3.77$	$\alpha = 0.29$, $\mu = 84.41$ $\hat{r} = 5.71$
ρ_2	$\alpha = 0.42$, $\mu = 22.58$ $\hat{r} = 2.80$	$\alpha = 0.36$, $\mu = 35.42$ $\hat{r} = 3.74$	$\alpha = 0.27$, $\mu = 78.67$ $\hat{r} = 5.62$

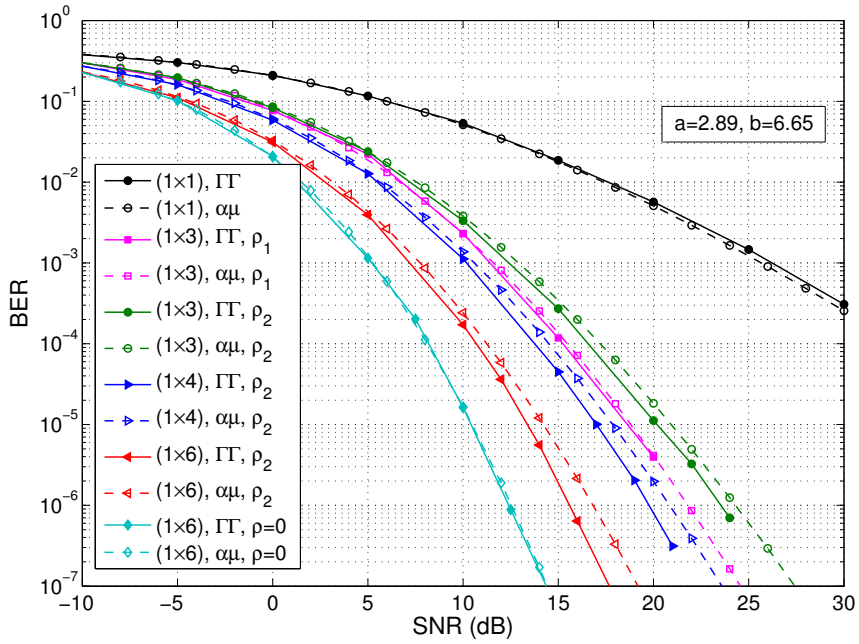

Figure 6. Contrasting BER performance obtained by Monte-Carlo simulation (using the ΓΓ model) and based on the α-μ approximation method.

5.2. Fading correlation effect on BER performance

We consider uncoded on-off keying modulation and the use of PIN photo-detectors at the receiver. Neglecting background radiations, we denote the variance of the receiver thermal noise by σ_n^2. EGC is performed on the received signals before demodulation assuming perfect channel knowledge. Considering $Z = 2\,\text{km}$ and $D_R = 50\,\text{mm}$ as before, we evaluate the average BER as a function of the average electrical signal-to-noise ratio (SNR). Considering a $(1 \times N)$ system, by approximating I_{sum} with R, the SNR after EGC is given by $\gamma_{\text{EGC}} \approx R^2/(4N\sigma_n^2)$, where we have set the optical-to-electrical conversion coefficient to unity. Then, the average BER can be calculated as [17]:

$$P_e \approx \frac{1}{2}\int_0^\infty p_R(r)\ \text{erfc}\left(\frac{r}{2\sqrt{2N}\sigma_n}\right)\,dr. \tag{9}$$

We have contrasted in Fig. 6 the BER performance obtained via Monte Carlo simulations based on the ΓΓ model and those obtained based on α-μ approximation from (9), where the average SNR for one branch is taken as the reference. For reference, we have also shown plots for the (1×1) system. Notice that we have generally a good agreement between the two sets of results. Although quite negligible, the difference is more considerable for larger ρ: for the (1×3) system, the SNR difference between the corresponding curves is around 0.05 and 0.75 dB at the target BER of 10^{-6} for the cases of ρ_1 and ρ_2, respectively. Meanwhile, we notice that there is a performance degradation

of about 2.1 dB at this BER from $\rho_1 = 0.12$ to $\rho_2 = 0.21$ (see [34] for a more detailed analysis of the effect of fading correlation on the system performance). We also have a larger difference for increased diversity order: it is about 1.1 and 1.2 dB for (1×4) and (1×6) systems, respectively, with ρ_2 at the BER of 10^{-6}. These results confirm those of KS test in Table 2(a). For the sake of completeness, we have also shown in Fig. 6 results for the (1×6) system with independent fading, where we notice an excellent match between the BER plots.

Lastly, it is worth mentioning that there is a practical limit on the number of apertures. This is because the relatively small performance improvement achieved cannot justify the increased receiver size and specially the system complexity and cost.

6. Conclusions

We investigated the fading correlation in space-diversity FSO systems. Considering the case study of a (1×3) system and realistic system parameters, we illustrated the effect of the link distance Z, receiver apertures' size D_R and aperture spacing Δ_C on the fading correlation. We showed that for relatively large Z, ρ depends mostly on the aperture edge separation Δ_E and is almost independent of D_R. On the other hand, in order to evaluate analytically the system performance under correlated fading conditions, we proposed to approximate the sum of arbitrarily correlated $\Gamma\Gamma$ RVs by an α-μ distribution. We verified the accuracy of this method by the KS statistic test and by contrasting the calculated BER performance with that obtained via Monte Carlo simulations based on the $\Gamma\Gamma$ model. Although we noticed a lower accuracy for increased correlation coefficient and diversity order, we showed that overall, the accuracy of the method is quite acceptable.

Acknowledgments

The authors would like to acknowledge the support by EU Opticwise COST Action IC1101. They also wish to thank Prof. Yahya Kemal Baykal from Çankaya University, Ankara, for the fruitful discussions on turbulence modeling. They are also thankful to Dr. Rausley Adriano Amaral de Souza from National Institute of Telecommunication, Minas Gerais, and Prof. Michel Daoud Yacoub from University of Campinas, São Paulo, Brazil, for discussions on the $\alpha - \mu$ approximation method.

Appendix: Derivation of third-order moment of correlated Gamma RVs

We explain here how to obtain the moment generating function (MGF) of multiple correlated Gamma RVs. Then, using this MGF, we derive the first three joint moments of L arbitrarily correlated Gamma RVs used in Subsection 3.2.

Lets consider the vector $\mathbb{W} = [W_1, W_2, \cdots, W_L]$, whose L elements are arbitrarily correlated but not necessarily identically distributed Gamma RVs, which have equal

shape and inverse scale parameters, denoted by m_1, m_2, ..., m_L, respectively. We also denote the auto-correlation matrix of $\mathbb{W}$ by $\mathbf{R}_{\mathbb{W}}$. Without loss of generality, we assume that the elements W_i are arranged in ascending order of their fading parameters, i.e., $1/2 \leqslant m_1 \leqslant m_2 \leqslant \cdots \leqslant m_L$. The MGF of $\mathbb{W}$, denoted by $\mathcal{M}_{\mathbb{W}}(\mathbf{s})$, can be expressed as [23]:

$$\mathcal{M}_{\mathbb{W}}(\mathbf{s}) = \mathcal{M}_{\mathbb{W}}(s_1, s_2, \cdots, s_L) = \prod_{i=1}^{L} \det(\mathbf{I} - \mathbf{S}_i \mathbf{A}_i)^{-n_i}, \tag{A.1}$$

where $\mathbf{I}$ represents an $(L \times L)$ Identity matrix and det(.) denotes matrix determinant. Also, $\mathbf{S}_1 = \mathbf{S}$ is a diagonal matrix of diagonal entries $s_1, s_2, \cdots, s_L$, denoted by $\text{diag}(s_1, s_2, \cdots, s_L)$. In addition, $\mathbf{A}_1 = \mathbf{A}$ is a positive-definite symmetric matrix that can be determined given m_i and $\mathbf{R}_{\mathbb{W}}$. Having $\mathbf{S}_1$ and $\mathbf{A}_1$, the other matrices $\mathbf{S}_i$ and $\mathbf{A}_i$ correspond to their lower $(L-i+1) \times (L-i+1)$ sub-matrices:

$$\mathbf{A}_i = \begin{pmatrix} A(i,i) & A(i,i+1) & \cdots & A(i,L) \\ \vdots & \vdots & & \vdots \\ A(L,i) & A(L,i+1) & \cdots & A(L,L) \end{pmatrix}, \tag{A.2}$$

where $A(p,q)$ is the (p,q)-th entry of $\mathbf{A}$, and

$$\mathbf{S}_i = \text{diag}(s_i, s_{i+1}, \cdots, s_L). \tag{A.3}$$

Also, n_i in (A.1) denotes the difference of the fading parameters, defined as:

$$n_i = \begin{cases} m_1, & i = 1 \\ m_i - m_{i-1}, & i = 2, 3, \cdots, L. \end{cases} \tag{A.4}$$

The first and the second moments of $\mathbb{W}$ are calculated in [23] and are presented below.

$$\mathrm{E}\{W_j\} = m_j A(j,j), \tag{A.5}$$

$$\begin{aligned} \mathrm{E}\{W_j W_k\} &= m_j m_k A(j,j) A(k,k) \\ &\quad + \min(m_j, m_k) A(j,k) A(k,j). \end{aligned} \tag{A.6}$$

For the moment matching method explained in Subsection 3.2, we also need the third moment of $\mathbb{W}$ that we calculate via the MGF $\mathcal{M}_{\mathbb{W}}(\mathbf{s})$. For this, we should first calculate the matrix $\mathbf{A}$ (and $\mathbf{A}_i$). Using (A.5) and (A.6), we can show that the correlation coefficient ρ_W^{jk} between W_j and W_k, which is the (j,k)-th entry of $\mathbf{R}_{\mathbb{W}}$, can be written as:

$$\rho_W^{jk} = \frac{\min(m_j, m_k)}{\sqrt{m_j m_k}} \frac{A^2(j,k)}{A(j,j)A(k,k)}. \tag{A.7}$$

Note that $A(\kappa, \tau) = A(\tau, \kappa)$ due to the symmetry of the correlation matrix. Then, to determine the matrix $\mathbf{A}$, the diagonal entries, e.g., $A(j,j)$, can be determined from $\mathrm{E}\{W_j\}$ from (A.5). Consequently, the entries $A(j,k)$ can also be determined from (A.7).

The joint moments of $\mathbb{W}$ can be directly calculated by taking the derivatives and partial derivatives of the MGF in (A.1) [38, Theorem 11.7]. To calculate the third

moment, let us start by giving the definitions of the first and second moments, given by (A.5) and (A.6), respectively. We have:

$$\frac{\partial \mathcal{M}_{\mathbb{W}}(\mathbf{s})}{\partial s_j} = \mathcal{M}_{\mathbb{W}}(\mathbf{s}) \sum_{i=1}^{j} n_i h_i(\mathbf{s}), \tag{A.8}$$

$$\begin{aligned}\frac{\partial^2 \mathcal{M}_{\mathbb{W}}(\mathbf{s})}{\partial s_j \partial s_k} = \frac{\partial \mathcal{M}_{\mathbb{W}}(\mathbf{s})}{\partial s_k} \sum_{i=1}^{j} n_i h_i(\mathbf{s}) \\ + \mathcal{M}_{\mathbb{W}}(\mathbf{s}) \sum_{i=1}^{\min(j,k)} n_i \frac{\partial h_i(\mathbf{s})}{\partial s_k},\end{aligned} \tag{A.9}$$

where $h_i(\mathbf{s})$ is defined as:

$$h_i(\mathbf{s}) = \mathrm{tr}\left\{ \left(\mathbf{I} - \mathbf{S}_i^T \mathbf{A}_i^T\right)^{-1} \left(\mathbf{E}_i(j,j)\mathbf{A}_i\right)^T \right\}, \tag{A.10}$$

where $\mathrm{tr}\{.\}$ denotes the trace of matrix, $(.)^T$ stands for transposition, and $\mathbf{E}_i(j,j)$ represents an $(L-i+1)\times(L-i+1)$ matrix specified below.

$$\mathbf{E}_i(j,j) = \mathrm{diag}(\underbrace{0,\cdots,0}_{j-i}, 1, \underbrace{0,\cdots,0}_{L-j}), j \geq i. \tag{A.11}$$

Also, the derivative of $h_i(\mathbf{s})$ is given as [23]:

$$\begin{aligned}\frac{\partial h_i(\mathbf{s})}{\partial s_k} = \mathrm{tr}\Big\{ \left(\mathbf{E}_i(j,j)\mathbf{A}_i\right) \\ \times \left[\left(\mathbf{I} - \mathbf{S}_i\mathbf{A}_i\right)^{-1} \left(\mathbf{E}_i(k,k)\mathbf{A}_i\right) \left(\mathbf{I} - \mathbf{S}_i\mathbf{A}_i\right)^{-1}\right] \Big\},\end{aligned} \tag{A.12}$$

Now, given the definition of the third moment:

$$\mathrm{E}\left\{W_j W_k W_l\right\} = \left.\frac{\partial^3 \mathcal{M}_{\mathbb{W}}(\mathbf{s})}{\partial s_j \partial s_k \partial s_l}\right|_{\mathbf{s}=0}, \tag{A.13}$$

we calculate the third order derivative as follows:

$$\begin{aligned}\frac{\partial^3 \mathcal{M}_{\mathbb{W}}(\mathbf{s})}{\partial s_j \partial s_k \partial s_l} = \frac{\partial^2 \mathcal{M}_{\mathbb{W}}(\mathbf{s})}{\partial s_k \partial s_l} \sum_{i=1}^{j} n_i h_i(\mathbf{s}) + \frac{\partial \mathcal{M}_{\mathbb{W}}(\mathbf{s})}{\partial s_k} \sum_{i=1}^{\min(j,l)} n_i \frac{\partial h_i(\mathbf{s})}{\partial s_l} \\ + \frac{\partial \mathcal{M}_{\mathbb{W}}(\mathbf{s})}{\partial s_l} \sum_{i=1}^{\min(j,k)} n_i \frac{\partial h_i(\mathbf{s})}{\partial s_k} + \mathcal{M}_{\mathbb{W}}(\mathbf{s}) \sum_{i=1}^{\min(j,k,l)} n_i \frac{\partial^2 h_i(\mathbf{s})}{\partial s_k \partial s_l}.\end{aligned} \tag{A.14}$$

Using some properties of matrix derivation from [39,40], we can obtain the second-order partial derivative of $h_i(\mathbf{s})$ as shown by (A.15) on the top of this page. In addition, we have:

$$\begin{cases} h_i(\mathbf{s})|_{\mathbf{s}=0} &= A(j,j), \\ \left.\frac{\partial h_i(\mathbf{s})}{\partial s_k}\right|_{\mathbf{s}=0} &= A(j,k)A(k,j), \\ \left.\frac{\partial^2 h_i(\mathbf{s})}{\partial s_k \partial s_l}\right|_{\mathbf{s}=0} &= A(j,l)A(l,k)A(k,j) \\ &+ A(j,k)A(k,l)A(l,j). \end{cases} \tag{A.16}$$

$$\frac{\partial^2 h_i(\mathbf{s})}{\partial s_k \partial s_l} = \mathrm{tr}\Big\{ \left(\mathbf{E}_i(j,j)\mathbf{A}_i\right)\left(\mathbf{I}-\mathbf{S}_i\mathbf{A}_i\right)^{-1}\left(\mathbf{E}_i(l,l)\mathbf{A}_i\right) \times \left(\mathbf{I}-\mathbf{S}_i\mathbf{A}_i\right)^{-1}\left(\mathbf{E}_i(k,k)\mathbf{A}_i\right)\left(\mathbf{I}-\mathbf{S}_i\mathbf{A}_i\right)^{-1} + \left(\mathbf{E}_i(j,j)\mathbf{A}_i\right)\left(\mathbf{I}-\mathbf{S}_i\mathbf{A}_i\right)^{-1}\left(\mathbf{E}_i(k,k)\mathbf{A}_i\right) \times \left(\mathbf{I}-\mathbf{S}_i\mathbf{A}_i\right)^{-1}\left(\mathbf{E}_i(l,l)\mathbf{A}_i\right)\left(\mathbf{I}-\mathbf{S}_i\mathbf{A}_i\right)^{-1} \Big\}. \quad \text{(A.15)}$$

Using (A.8)-(A.16), the general from of third moment is obtained as

$$\begin{aligned}
&\mathrm{E}\left\{W_j W_k W_l\right\} = \left.\frac{\partial^3 \mathcal{M}_{\mathbb{W}}(\mathbf{s})}{\partial s_j \partial s_k \partial s_l}\right|_{\mathbf{s}=0} \\
&= m_j m_k m_l A(j,j)A(k,k)A(l,l) \\
&+ m_j A(j,j)\min(m_k,m_l)A^2(k,l) \\
&+ m_k A(k,k)\min(m_l,m_j)A^2(l,j) \\
&+ m_l A(l,l)\min(m_j,m_k)A^2(j,k) \\
&+ 2\min(m_j,m_k,m_l)A(j,k)A(k,l)A(l,j). \qquad \text{(A.17)}
\end{aligned}$$

Other third-order joint moments can be calculated from this general equation. For instance, to calculate $\mathrm{E}\left\{W_j^2 W_k\right\} = \mathrm{E}\left\{W_j W_j W_k\right\}$, we should just set $k = j$ and $l = k$ in (A.17).

References

[1] Z. Ghassemlooy, W. Popoola, and S. Rajbhandari. *Optical Wireless Communications: System And Channel Modelling With* MATLAB. CRC Press, Boca Raton, FL, 2013.

[2] L. C. Andrews and R. L. Phillips. *Laser Beam Propagation Through Random Media*. SPIE Press, 2nd edition, 2005.

[3] E. J. Lee and V. W. S. Chan. Part 1: Optical communication over the clear turbulent atmospheric channel using diversity. *IEEE Journal on Selected Areas in Communications*, 22(9):1896–1906, Nov. 2004.

[4] S. G. Wilson, M. Brandt-Pearce, Q. L. Cao, and M. Baedke. Optical repetition MIMO transmission with multipulse PPM. *IEEE Journal on Selected Areas in Communications*, 23(9):1901– 1910, Sep. 2005.

[5] M. A. Khalighi, N. Schwartz, N. Aitamer, and S. Bourennane. Fading reduction by aperture averaging and spatial diversity in optical wireless systems. *IEEE/OSA Journal of Optical Communications and Networking*, 1(6):580–593, Nov. 2009.

[6] J. A. Anguita, M. A. Neifeld, and B. V. Vasic. Spatial correlation and irradiance statistics in a multiple-beam terrestrial free-space optical communication link. *Applied Optics*, 46(26):6561–6571, Sep. 2007.

[7] F. D. Kashani, M. R. H. Rad, Z. Firozzadeh, and M. R. Mahzoun. Beam propagation analysis of a multi-laser diode FSO system through free space. *Journal of Optics*, 13(10):105709, Oct. 2011.

[8] S. M. Navidpour, M. Uysal, and M. Kavehrad. BER performance of free-space optical transmission with spatial diversity. *IEEE Transactions on Wireless Communications*, 6(8):2813–2819, Aug. 2007.

[9] N. Letzepis, I. Holland, and W. Cowley. The Gaussian free space optical MIMO channel with Q-ary pulse position modulation. *IEEE Transactions on Wireless Communications*, 7(5):1744–1753, May 2008.

[10] Z. Chen, S. Yu, T. Wang, G. Wu, S. Wang, and W. Gu. Channel correlation in aperture receiver diversity systems for free-space optical communication. *Journal of Optics*, 14(12):125710, Dec. 2012.

[11] X. M. Zhu and J. M. Kahn. Free-space optical communication through atomospheric turbulence channels. *IEEE Transactions on Communications*, 50(8):1293–1300, Aug. 2002.

[12] M. Uysal, S. M. Navidpour, and J. Li. Error rate performance of coded free-space optical links over strong turbulence channels. *IEEE Communications Letters*, 8(10):635–637, Oct. 2004.

[13] N. D. Chatzidiamantis and G. K. Karagiannidis. On the distribution of the sum of Gamma-Gamma variates and applications in RF and optical wireless communications. *IEEE Transactions on Communications*, 59(5):1298–1308, May 2011.

[14] K. P. Peppas. A simple, accurate approximation to the sum of Gamma-Gamma variates and applications in MIMO free-space optical systems. *IEEE Photonics Technology Letters*, 23(13):839–841, July 2011.

[15] J. A. Tellez and J. D. Schmidt. Multiple transmitter performance with appropriate amplitude modulation for free-space optical communication. *Applied Optics*, 50(24):4737–4745, Aug. 2011.

[16] K. P. Peppas, G. C. Alexandropoulos, C. K. Datsikas, and F. I. Lazarakis. Multivariate Gamma-Gamma distribution with exponential correlation and its applications in radio frequency and optical wireless communications. *IET Microwaves, Antennas & Propagation*, 5(3):364–371, Feb. 2011.

[17] G. Yang, M. A. Khalighi, S. Bourennane, and Z. Ghassemlooy. Approximation to the sum of two correlated Gamma-Gamma variates and its applications in free-space optical communications. *IEEE Wireless Communications Letters*, 1(6):621–624, Dec. 2012.

[18] J. H. Churnside. Aperture averaging of optical scintillations in the turbulent atmosphere. *Applied Optics*, 30(15):1982–1994, May 1991.

[19] L. C. Andrews, R. L. Phillips, and C. Y. Hopen. *Laser Beam Scintillation with Applications*. SPIE Press, Bellingham, Washington, 2001.

[20] D. L. Hutt. Modeling and measurements of atmospheric optical turbulence over land. *Optical Engineering*, 38(8):1288–1295, Aug. 1999.

[21] D. H. Tofsted, S. G. O'Brien, and G. T. Vaucher. An atmospheric turbulence profile model for use in army wargaming applications I. Technical Report ARL-TR-3748, Army Research Laboratory, White Sands Missile Range, NM, Feb. 2006.

[22] G. Yang, M. A. Khalighi, and S. Bourennane. Performance of receive diversity FSO systems under realistic beam propagation conditions. *IEEE, IET Int. Symposium on Communication Systems, Networks and Digital Signal Processing (CSNDSP)*, pages 1–5, July 2012. Poznan, Poland.

[23] Q. T. Zhang. A generic correlated Nakagami fading model for wireless communications. *IEEE Transactions on Communications*, 51(11):1745–1748, 2003.

[24] J. D. Schmidt. *Numerical Simulation of Optical Wave Propagation With Examples in MATLAB*. SPIE Press, 2010.

[25] E. W. Stacy. A generalization of the Gamma distribution. *The Annals of Mathematical Statistics*, 33(3):1187–1192, Sept. 1962.

[26] M. D. Yacoub. The α-μ distribution: A physical fading model for the stacy distribution. *IEEE Transactions on Vehicular Technology*, 56(1):27–34, Jan. 2007.

[27] M. Safari and M. Uysal. Do we really need OSTBCs for free-space optical communication with direct detection? *IEEE Transactions on Wireless Communications*, 7(11):4445–4448, Nov. 2008.

[28] G. Yang, M.-A. Khalighi, T. Virieux, S. Bourennane, and Z. Ghassemlooy. Contrasting space-time schemes for MIMO FSO systems with non-coherent modulation. *International Workshop on Optical Wireless Communications (IWOW)*, Oct. 2012. Pisa, Italy.

[29] M. Abramowitz and I. A. Stegun, editors. *Handbook of Mathematical Functions with Formulas, Graphs, and Mathematical Tables*. Dover Publications, June 1965.

[30] F. S. Vetelino, C. Young, L. C. Andrews, and J. Recolons. Aperture averaging effects on the probability density of irradiance fluctuations in moderate-to-strong turbulence. *Applied Optics*, 46(11):2099–2108, Apr. 2007.

[31] A. D. Wheelon. *Electromagnetic Scintillation: Volume 2, Weak Scattering*. Cambridge University Press.

[32] A. Papoulis and S. U. Pillai. *Probability, Random Variables and Stochastic Processes*. McGraw-Hill, 4th edition, 2001.

[33] N. Zlatanov, Z. Hadzi-Velkov, and G. K. Karagiannidis. An efficient approximation to the correlated Nakagami-m sums and its application in equal gain diversity receivers. *IEEE Transactions on Wireless Communications*, 9(1):302–310, May 2010.

[34] G. Yang, M. A. Khalighi, Z. Ghassemlooy, and S. Bourennane. Performance evaluation of receive-diversity free-space optical communications over correlated gamma-gamma fading channels. *Applied Optics*, 52(24):5903–5911, Aug. 2013.

[35] Q. T. Zhang. A decomposition technique for efficient generation of correlated Nakagami fading channels. *IEEE Journal on Selected Areas in Communications*, 18(11):2385–2392, Nov. 2000.

[36] M. K. Simon and M.-S. Alouini. *Digital communication over fading channels*. Wiley-Interscience, New York, 1st edition, July 2000.

[37] G. C. Alexandropoulos, N. C. Sagias, F. I. Lazarakis, and K. Berberidis. New results for the multivariate Nakagami-m fading model with arbitrary correlation matrix and applications. *IEEE Transactions on Wireless Communications*, 8(1):245–255, Jan. 2009.

[38] A. DasGupta. *Fundamentals of Probability: A First Course*. Springer Texts in Statistics. Springer, New York, 1st edition, Apr. 2010.

[39] D. Zwillinger. *CRC Standard Mathematical Tables and Formulae*. Chapman and Hall/CRC, New York, 31st edition, Nov. 2002.

[40] K. B. Petersen and M. S. Pedersen. *The Matrix Cookbook*. Technical University of Denmark, Nov. 2012. [Online]. Available: http://www2.imm.dtu.dk/pubdb/p.php?3274.